Shear banding leads to accelerated aging dynamics in a metallic glass

Stefan Küchemann, Chaoyang Liu, Eric M. Dufresne, Jeremy Shin, and Robert Maaß

Phys. Rev. B **97**, 014204 — Published 11 January 2018

DOI: 10.1103/PhysRevB.97.014204

Shear banding leads to accelerated aging dynamics in a metallic glass

Stefan Küchemann[1], Chaoyang Liu[1], Eric M. Dufresne[2], Jeremy Shin[1], Robert Maaß[1*]

[1] Department of Materials Science and Engineering and Frederick-Seitz Materials Research Laboratory, University of Illinois at Urbana-Champaign, Urbana, IL 61801, USA

[2] Advanced Photon Source, Argonne National Laboratory, Lemont, IL 60439, USA

* rmaass@illinois.edu

Abstract

Traditionally, strain localization in metallic glasses is related to the thickness of the shear defect, which is confined to the nanometer scale. Using site-specific x-ray photon correlation spectroscopy (XPCS), we reveal significantly accelerated relaxation dynamics around a shear band in a metallic glass at a length scale that is orders of magnitude larger than the defect itself. The relaxation time in the shear-band vicinity is up to ten-times smaller compared to the as-cast matrix, and the relaxation dynamics occurs in a characteristic three-stage aging response that manifests itself in the temperature-dependent shape parameter known from classical stretched exponential relaxation dynamics of disordered materials. We demonstrate that the time-dependent correlation functions describing the aging at different temperatures can be captured and collapsed using simple scaling functions. These insights highlight how an ubiquitous nano-scale strain-localization mechanism in metallic glasses leads to a fundamental change of the relaxation dynamics at the mesoscale.

I. Introduction

Like many other amorphous materials, metallic glasses (MGs) yield under an external stress via a strain-localization mechanism, forming thin layers of deforming material that are referred to as shear bands [1-5]. Shear bands in MGs mediate plastic deformation, but also promote structural collapse via a shear-band-to-crack transition, which has hampered the success of MGs as an engineering material. In contrast to other amorphous systems with much larger particle size, such as granular materials, it remains a fundamental challenge to track structural changes in the atomically disordered MG. This also applies to shear bands, even though advanced electron microscopy techniques are able to reveal their structural signature in contrast to the surrounding matrix [6-8]. One long-standing figure of merit that characterizes the shear band is its thickness that often is assumed to be ca. 10-20 nm [2,9,10], but which recently was shown to be position dependent and ranging between ca. 10-200 nm [10]. Into this narrow layer, all structural degradation is believed to be imparted. Here we show evidence that this is not the case. Instead, we reveal with site-specific x-ray photon correlation spectroscopy (XPCS), that the shear-band significantly alters the glassy material at a length-scale that is approximately three orders of magnitude larger than typically considered. It is found that the nano-scale core of a shear band promotes 10 times faster relaxation dynamics in the surrounding matrix, and that an accelerated aging exhibits a distinct three-stage behavior if compared to the unbiased matrix. We describe the different aging regimes with simple scaling functions that distinguishes the deformation-induced structural dynamics from the simple aging behavior of the as-cast MG. The implication of this fundamental insight is that structural degradation due to shear bands is far from limited to the nanometer scale, urging to revise our view on strain localization in MGs.

The understanding of shear-band formation and structure plays a crucial role in both the development of a fundamental theory of plastic deformation and in determining a specific metallic-glass alloy's performance in structural applications. Despite the long research history dedicated to shear bands in MGs, progress is slow, with recent experimental focus on the structural state of existing shear bands [2,6-8,10-13], the formation mechanism [14,15] or the macroscopic-dynamic response of active shear bands during deformation [5,16-22].

A number of mechanisms have been explored for shear-band formation in MGs [23-27]. Based on molecular dynamics (MD) simulations, Cao et al. attribute the origin of shear-band formation to a cascade of structural instabilities starting from the disruption of an icosahedral cluster, which leads to disorder-induced softening followed by thermal softening [27]. On mesoscopic length scales the initial stage of shear-band formation was attributed to a spatial clustering of shear-transformation-zone nucleation sites [23], which is impaired by the

initial concentration of quasi-crystalline short range order [24]. Despite these valuable insights from computer simulations, the experimental validation of a local dilatation and consequent softening during shear-band formation is not straightforward and remains a topic of intense research efforts [28-30]. Relying on an experimental waiting time analysis, the precursor activity to shear-band formation has been associated to a transition from a three dimensional uncorrelated activation to a correlated alignment of shear transformation zones into a two dimensional shear-plane [31,32]. The believed shear dilatation at the onset of strain localization is sought to generate a free volume increase in the nanometer thick shear band and was quantified by means of in-situ acoustic emission experiments to a maximum of ca. 8.5%, with a median around 2% [14]. Even after unloading, the free volume change remains, thus forming a traceable contrast from the surrounding amorphous matrix that can be visualized with transmission electron microscopy (TEM). Indeed, recent studies of post-mortem shear bands determined the density change in a shear band to be between -12% and +6% [7,10]. Since the shear band predominantly shows a zone of decreased density, strongly facilitated diffusion [33] that potentially leads to crystallization [6,11] may be observed.

The aforementioned reports have in common that they rely on the concept of an isolated nano-scale sheared zone, without attributing any effects to the surrounding matrix. More recent studies have revealed that the picture of a shear band requires a more complex view, where the shear defect has a nano-scale core and some yet unclear long-range zone [34,35]. For example, using large area nano-indentation mapping it was demonstrated that the surrounding matrix exhibits position-dependent fluctuations of hardness, which may be ascribed to the presence of long-range internal stress fields formed around the shear band [35]. Mapping local strain fields also revealed strain fluctuations beyond the shear-band itself, both at the sub-micron scale [36] and micron scale [37]. These finding introduce a concept of complex internal length scales that can be of the scale up to hundreds of micrometers in addition to the nano-scale core, which was subsequently supported in nano-beam x-ray diffraction measurements [38]. These developments suggest that even after the dissipative shear event when the material is in an unloaded state, the MG-matrix surrounding the shear-band core is fundamentally biased and different dynamics of the glassy material may be expected. This hypothesis forms the basis of the present work.

An experimental method that allows quantitative insights into atomic-scale structural relaxation dynamics is x-ray photon correlation spectroscopy (XPCS) [39]. Evaluating time and temperature-dependent intensity fluctuations, XPCS is capable of revealing clear differences in the decay of the intensity correlation functions obtained for the glassy-solid and the supercooled-liquid state [40]. While the supercooled metallic-glass-forming liquid describes a stretched exponential decorrelation, well known from equilibrated Lennard-Jones glasses, Van-der-Waals liquids, network and ionic glass forming liquids [41-43], the solid structure below the glass transition

temperature, exhibits a compressed exponential decorrelation [40] that resembles out-of-equilibrium dynamics of colloidal gels and nano-particles [44-47]. This transition in the exponent (shape parameter) of the exponential decorrelation from a stretched (<1) to a compressed (>1) exponential decay of the correlation function was previously associated with the difference in the underlying mechanism of structural relaxation, which changes from a diffusive behavior in the supercooled liquid to a stress relaxation dominated behavior in the solid glass state [40].

Using site-specific XPCS, we show here that the structural relaxation dynamics, characterized by a relaxation time, in the material surrounding the shear band is up to one order of magnitude faster than in the undeformed bulk. This difference persists up to elevated temperatures close to the glass transition temperature, evidencing that thermal excitation does not erase the deformation history immediately reflected by the relaxation time. Consequently, enhanced relaxation and, potentially, structural changes do not only occur in the nano-scopic shear-band core, but also in its surroundings on a length scale of tens of micrometers. We interpret our findings based on a medium-range ordering mechanism as the first step in the equilibration process of the shear-band zone (not core) in comparison to the undeformed bulk. This process is likely due to the reformation of icosahedral clusters and a network thereof, which are known to be disrupted during the strain localization event. We are furthermore able to quantify the underlying aging dynamics around the shear-band core by scaling the intensity correlation functions for different waiting times at one temperature, thereby showing a crossover in the sub-aging regime from an exponential to a logarithmic scaling.

II. Experimental techniques

A. Sample preparation

Raw materials were purchased from Alfa Aesar with a purity of Zr 99.8% (metal basis), Cu 99.9999% (metal basis) and Al 99.9999% (metals basis). Bulk metallic glass rods (length = 3 mm, diameter = 2 mm) made of $Zr_{65}Cu_{25}Al_{10}$ were prepared via suction casting using an arc melter of type MAM1 from Edmund Bühler GmbH 240 days prior to the measurements. All reported data for the as-cast reference state were obtained from a specimen produced according to this standard procedure. The amorphous structure of all cast samples was verified via wide angle x-ray diffraction using a Philips Xpert 2 with a combination of two wavelengths in the ratio 1:1, Cu $K_{\alpha,1}$ with λ_1 = 1.5406 Å and Cu $K_{\alpha,2}$ with λ_2 = 1.5444 Å. The MG rods were notched at a 45° angle using electric discharge machining in order to generate a single system-spanning shear band that admitted all macroscopic plastic strain during deformation. Several samples were deformed at -40 °C to a total compressive strain of 10% using an Instron

testing rig 5900r 10 days before the measurements. Both the as-cast and deformed cylindrical samples were polished according to the procedure outlined in Ref. [35]. Polishing was done such that flat surfaces parallel to the cylindrical rod axis were created, also assuring that the shear plane is approximately normal to the polished surfaces. In the following, we report on x-ray data from one as-cast reference sample and one deformed and polished specimen.

B. X-ray photon correlation spectroscopy measurements

X-ray photon correlation spectroscopy (XPCS) measurements were performed at beamline 8-ID-E of the Advanced Photon Source at Argonne National Laboratory at an energy of $E = 7.35$ keV in reflection geometry (Fig. 1a). Samples were heated stepwise in vacuum until the glass transition temperature at around 570 K. The temperature was held constant for a certain amount of time, beginning with 4 hours at room temperature and this measurement time interval was successively decreased to a 20 min measurement time close to the glass transition temperature. Note that the glass transition temperature is significantly shifted to lower temperatures in comparison to the calorimetric glass transition temperature around 636 K due to the very low heating rates (for an estimate of the heating-rate-dependent shift of the glass transition temperature we refer to Ref. [48]). The coherent beam had a size of 10×7 μm². Under a scattering angle of $\theta = 20°$ between the incoming beam and the sample surface, this beam size probes an area of 10 x 20.47 μm² on the sample, which significantly exceeds the nanoscale spatial scale of a shear band in a MG. The scattered beam was recorded using a charged coupled device (CCD) camera with an exposure time of 10 s. Several cavities were identified along the shear-band path. These macroscopic regions of delamination on the shear plane mark a shear-band-to-crack transition and have been revealed in our earlier work [10,34,35]. They allow tracing of the shear band, since they form a visible contrast in both optical/electron microscopy as well as x-ray diffraction maps (Fig. 1b-c). For the XPCS measurements, we chose a location along the shear-band path that was about 10 μm away from a cavity to assure that the obtained data originates from a sampled volume around the shear-band core. After thermal equilibration at each temperature, the beam location on the sample surface was re-adjusted via x-ray diffraction mapping (Fig. 1b) in order to record the relaxation data from the same location on the sample surface. Using knife-edge scans and the sample dimensions, the incident-beam location near the cavity was confirmed.

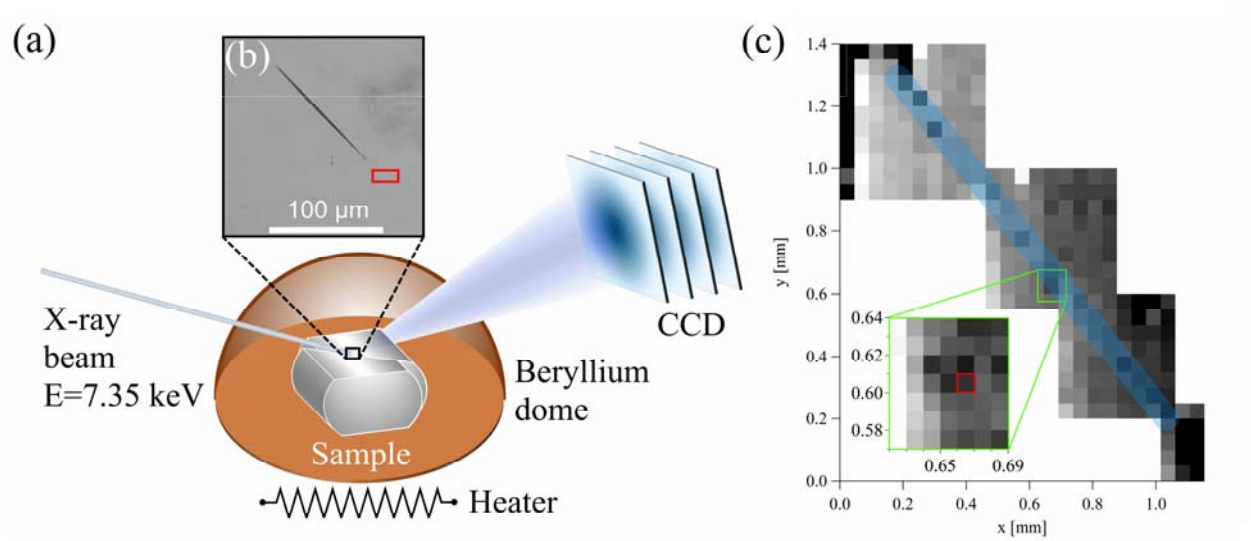

Fig. 1. (a) Schematic representation of the scattering setup. (b) Optical micrograph magnification of the cavity, including the x-ray probe location in red. (c) Intensity map of the first peak of the structure factor along the shear band. The light blue region highlights the shear band path. The inset in (c) represents a zoom-in of the region around the cavity with the probe location marked in red.

C. Error determination of collapsed correlation functions

In the forthcoming discussion section, correlation functions at different waiting times are collapsed onto each other, and the quality of the collapse is evaluated. The best collapse of the correlation functions of different ages at a given temperature (Fig. 6, Section IV.B) was identified via minimization of the variance $V(\Delta t)$ with

$$\Delta t = \log\left\{\tau \cdot \left[\ln\left(\frac{g_2(t)-1-y_0}{B}\right)\right]^{1/\beta}\right\} - \log\{t\} \tag{5}$$

For the variance $V(\Delta t)$, the input parameters, τ, β, B and y_0, were determined via the compressed exponential fit $f(x) = y_0+B\cdot exp(-2\cdot(x/\tau)^{\beta})$ including all data points from the correlation functions g_2-1 of all ages which were considered for the collapse. Therefore, the values Δt correspond to the horizontal difference in Fig. 6a-d between the data points and the fit $f(x)$ on a logarithmic scale.

III. Results

A. Time-averaged relaxation dynamics

Speckle patterns from the as-cast and the deformed sample were recorded at a scattering angle of 2θ = 40.4° (q = 2.59 Å^{-1}), which corresponds to the maximum of the structure factor of $Zr_{65}Cu_{25}Al_{10}$ (glass transition temperature, T_g = 570 K). The probe location on the deformed sample was positioned close to a cavity that unambiguously defines the shear-band path [10,35] (Fig. 1a and 1b). Fig. 1c displays the intensity of the first peak of the structure factor in real-space coordinates across the sample. A faint contrast indicates the shear-band line (highlighted in light blue), and the zoom-in marks the location of the incident x-ray beam.

Time-resolved speckle patterns were recorded during isothermal steps in the heating process and the intensity correlation function

$$g_2(t) = \frac{\left\langle \left\langle I_p(t_w) I_p(t_w + t) \right\rangle_{t_w} \right\rangle_p}{\left\langle \left\langle I_p(t_w) \right\rangle_{t_w}^2 \right\rangle_p} \qquad (1)$$

was evaluated, where t_w here indicates the starting time of the measurement, I_p denotes the intensity in the detector pixel p, $\langle \ldots \rangle_p$ corresponds to the ensemble average of all pixel with the same scattering vector q, and $\langle \ldots \rangle_{t_w}$ represents the time average [49]. The change of g_2-1 as a function of time at different temperatures for the as-cast sample is displayed in Fig. 2a. At every temperature studied, the correlation function g_2-1 exhibits a complete decay to zero, showing that even at room temperature the structure of the as-cast MG is not frozen, but undergoes significant structural relaxation.

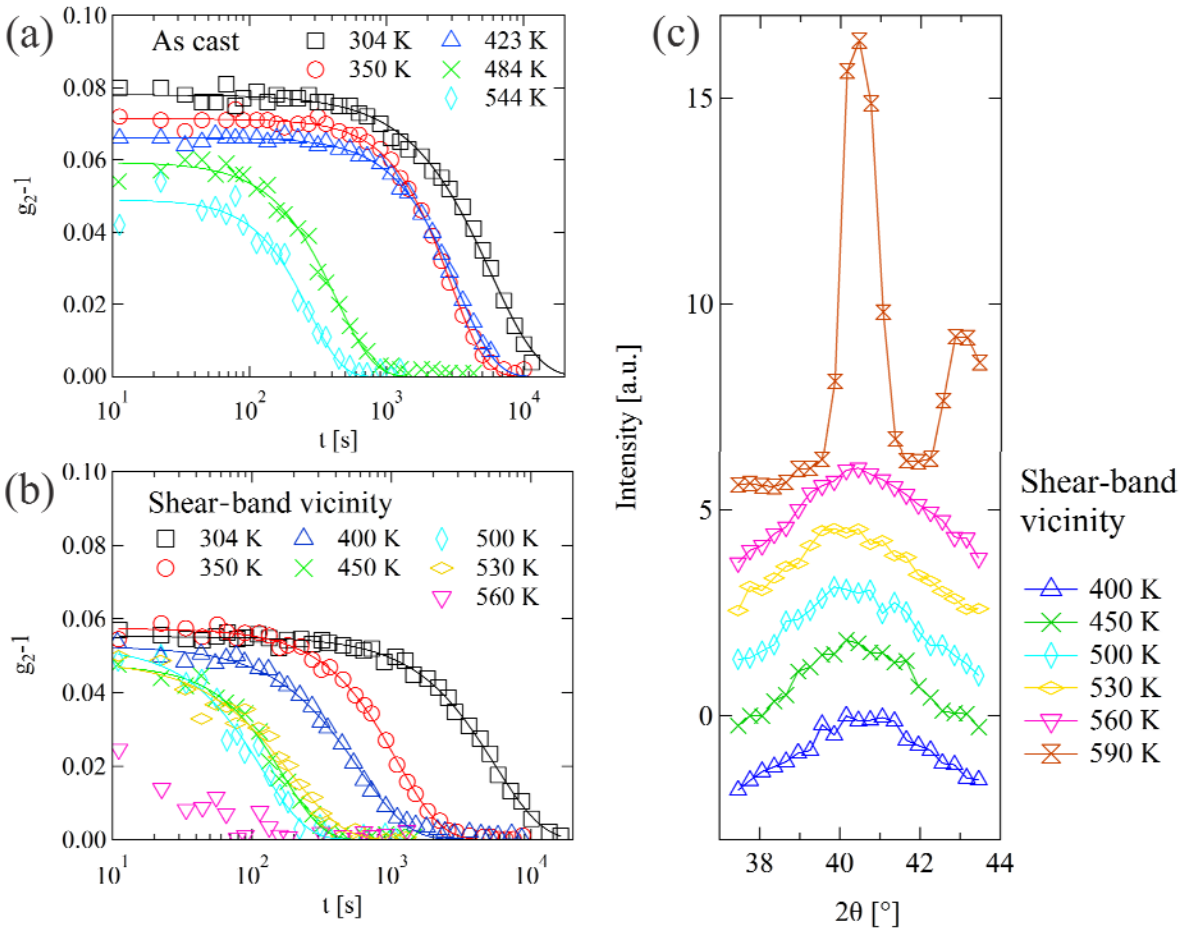

Fig. 2. Correlation functions of the undeformed amorphous matrix (panel (a)) and the shear band region (panel (b)) at various temperatures below the glass transition temperature of 570 K. (c) shows a 2θ scan data over an angular range of 27° to 44°, indicating that crystallization of the probed material in the shear-band region first occurs at 590 K. The 2θ scan was conducted after the relaxation dynamics was probed at each temperature step.

Figure 2b shows the correlation function at various temperatures for the probed material of the shear-band zone. At elevated temperatures, the decay of the correlation function occurs on shorter timescales and reaches the temporal resolution limit at 560 K. In the subsequent analysis and discussions, 560 K will therefore be omitted. The material around the shear-band core exhibits qualitatively the same behavior as the as-cast reference, with a complete decay at every studied temperature within the investigated time window. However, the decay of g_2-1 is significantly earlier along the time-axis. In order to verify that we are probing an amorphous structure throughout all temperature steps in our XPCS experiments, a 2θ-scan covering 37-44° was conducted after each temperature step. This temperature range includes the first broad peak of the MG, as well as positions of Bragg reflections from crystalline phases of the studied alloy. The resulting data is summarized in Fig. 2c, clearly demonstrating that

crystallization first occurs at 590 K, which is a temperature that is not further considered in the following XPCS analysis.

The decay of the correlation function can be quantified with a stretched exponential Kohlrausch-Williams-Watts (KWW) function [50]:

$$g_2 - 1 = g_{2,plat} \cdot \exp(-2 \cdot (t/\tau_\alpha)^\beta) \quad (2)$$

where β refers to the shape parameter (β = 1 means a standard exponential decay, β < 1 indicates a stretched exponential decay and β > 1 signifies a compressed exponential decay), τ_α is the relaxation time, and $g_{2,plat}$ corresponds to the value of the short-time plateau ($g_2(t = 0)$). $g_{2,plat}$ is the product between an experimental contrast value and the square of the Debye-Waller factor. In our measurements in reflection geometry, the g_2-1 of 8% is slightly higher than previously reported values of 4% [40] and 6% [51] for MGs probed in transmission geometry. In a quantitative comparison between the as-cast glass and the region around the shear-band core, the relaxation time in both regions (Fig. 3a) exhibits a temperature-dependent decrease, as expected from Fig. 2. However, the relaxation time is up to one order of magnitude smaller in the vicinity of the shear-band core as compared to the undeformed bulk, which is in qualitative agreement with reported enhanced relaxation dynamics in deformed Pd-based MGs [52]. This enhanced relaxation behavior is also apparent in the value of the initial plateau $g_{2,plat}$ (Fig. 3b), which is significantly smaller near the shear-band core at temperatures below 450 K. Above this temperature, $g_{2,plat}$ suddenly starts to increase, finally reaching the value of the undeformed bulk that has a monotonically decaying $g_{2,plat}$. As such, the $g_{2,plat}$ value can be used as an indicator for when the material around the shear-band core starts to become indistinguishable from the undeformed bulk due to progressing relaxation.

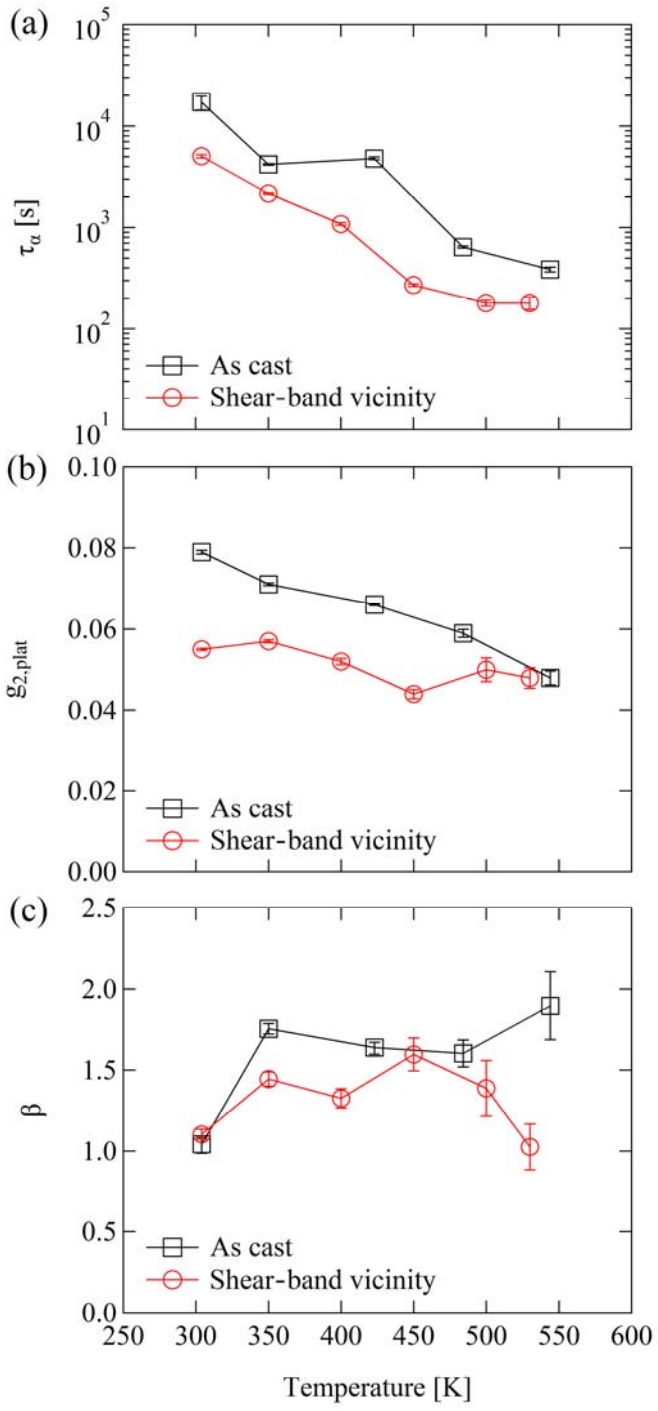

Fig. 3. (a) relaxation time τ_α, (b) $g_{2,plat}$ and (c) the shape parameter β

The evaluation of the shape parameter reveals overall a similar behavior as the other two fitting parameters, with an offset of the shear-band affected zone to lower values (Fig. 3c). The shape parameter in the unbiased matrix exhibits an approximate constant level of $\beta > 1$ for all temperature greater than 304 K, which corresponds to a compressed exponential response. A shape parameter much larger than one, ranging between ca. 1.2 and 2 has

reported for as-cast Zr-, Pd- and Mg-based MGs [40,51,53], and was attributed to an internal stress-relaxation response, which is different than the expected diffusive behavior in the supercooled liquid [40]. As pointed out earlier [53], such high values are not in agreement with current theories on dynamics in the glassy state [54]. At 304 K, β is also approximately 1 for the shear-band affected zone. With increasing temperature, the shape parameter gradually reaches a maximum at 450 K, where its value is close to the one of the as-cast material. While the shape parameter of the material around the shear-band core clearly decays to 1 upon heating further above 450 K, no temperature-dependent decay of β is seen for the as-cast material up to the highest temperature (ca. $0.95\times T_g$). Based on earlier results [40], a reduction close to T_g may be expected, but yet other measurements revealed significant fluctuations in β near the glass transition from the TTCF [55].

B. Momentary relaxation dynamics

In addition to the global decay of the intensity correlation function, a more detailed view on the glassy dynamics can be obtained by evaluating the two-time correlation function (TTCF) [44]:

$$C(t_1,t_2)=\frac{\left\langle I_p(t_1)I_p(t_2)\right\rangle_p}{\left\langle I_p(t_1)\right\rangle_p\left\langle I_p(t_2)\right\rangle_p}\ , \tag{3}$$

which is similar to equation (1) with the difference that the correlation function C in equation (3) represents a cross correlation of intensities at two times t_1 and t_2. Therefore it is possible to evaluate the momentary relaxation behavior at different time steps for a given temperature and to observe the aging behavior. Fig. 4 shows the TTCF of the as-cast sample ((a)-(c)) and the material around the shear-band core ((d)-(f)) at different temperatures. The TTCF in both regions clearly broadens below 423 K due to aging. Even at room temperature, the as-cast matrix shows a clear signature of aging and therefore structural dynamics. Both regions depict a steady state regime above 530 K, during which the TTCF does not broaden and the momentary relaxation time, $\tau_{\alpha,m}$, indicated by the vertical distance of the diagonal to the upper red line (or the horizontal distance to the lower red line) remains constant. The relaxation time evaluated along the diagonal trace also displays some intermittent behavior which was previously attributed to intermittent aging dynamics [55].

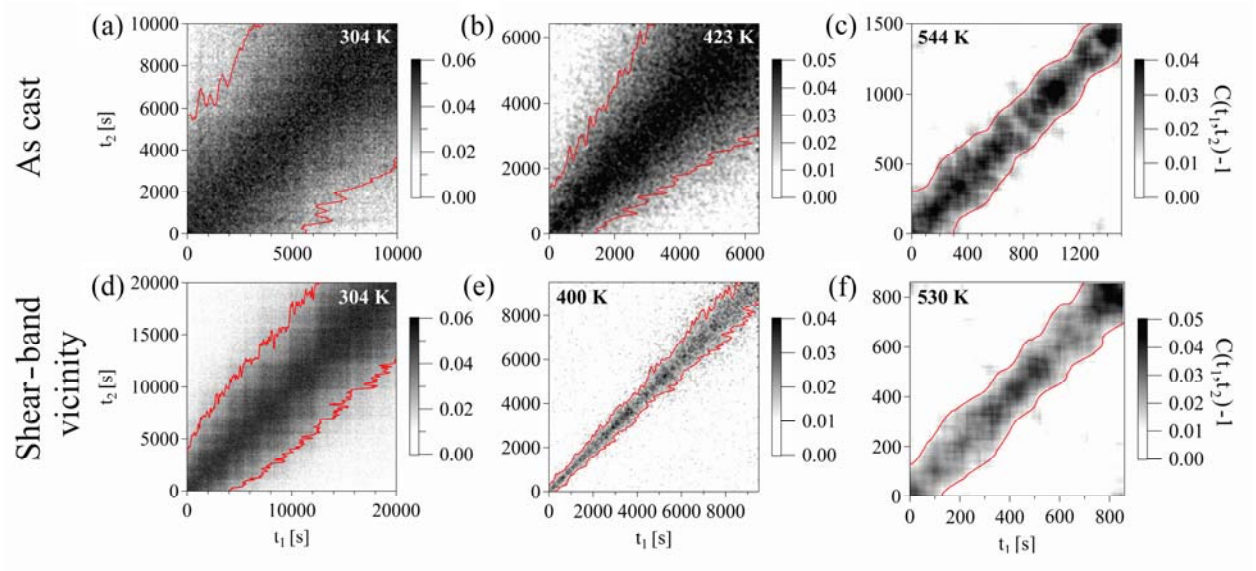

Fig. 4. Two-time correlation functions of the as cast state (top row, panels (a)-(c)) and in the material around the shear-band core (bottom row, panels (d)-(f)) at various temperatures. The red line indicates the time when $C(t_1,t_2)$-1 decayed to 1/e. Therefore, the horizontal distance from the diagonal to the lower red line (or vertical distance from the diagonal to the upper red line) corresponds to the momentary relaxation time $\tau_{\alpha,m}$.

In order to quantitatively evaluate the broadening of the TTCF, we extract $\tau_{\alpha,m}$ at different times of the experiment. This is done by evaluating time traces, i.e. horizontal lines between the diagonal and the point at which it has decayed to 1/e indicated by the red line, in the TTCF. Fig. 5 shows the change of the momentary relaxation time as a function of waiting time t_w in the as-cast matrix (panel (a)) and around the shear-band core (panel (b)). Note that the value of the waiting time is given with respect to the start of the measurement, meaning that the time elapsed between casting the samples, the deformation experiment, and the X-ray experiments was not accounted for. In contrast to earlier findings [40], Fig. 5 reveals that the graphs of the relaxation time for different temperatures of both glassy states do not collapse to a master curve by normalizing the ordinate with the initial relaxation time τ_0. In the undeformed matrix, the instantaneous relaxation time at temperatures below 423 K exhibits an increase within the examined time interval. This type of aging is called sub-aging, i.e. the relaxation time increases more slowly than the waiting time [56], corresponding to a slope below unity of the data in Fig. 5. At higher temperatures, the relaxation time remains constant and hence does not show any sign of aging or sub-aging. Around the shear-band core the relaxation time increases with a progress in waiting time at all temperatures up to 450 K. In contrast, the as-cast matrix does not evidence any further aging above $T = 423$ K. Below 450 K the shear-band zone undergoes sub-aging, and at room temperature the relaxation time grows markedly slower than at higher temperatures. The room-

temperature behavior indicates a clear deviation at long waiting times away from the relaxation-time increase observed at higher temperatures. This indicates that the aging behavior at 304 K has already slowed down, which is likely due to the long exposure to ambient conditions before the start of the x-ray measurements.

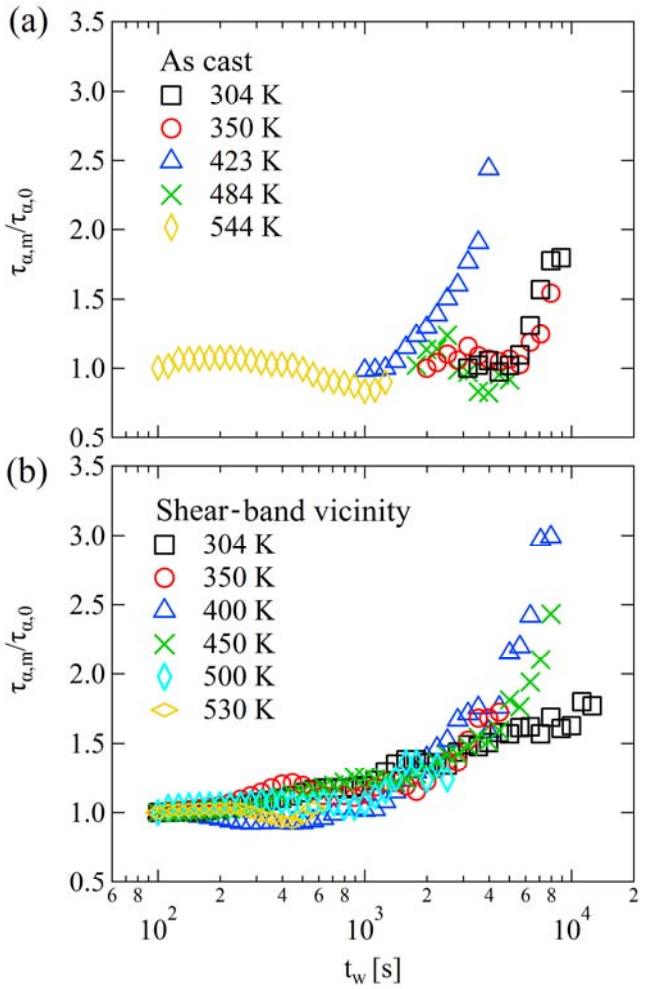

Fig. 5. (a) Momentary relaxation time $\tau_{\alpha,m}$ as a function of waiting time t_w.in the as cast state and (b) in the shear–band affected zone at various temperatures.

IV. Discussion

The data presented here highlights the importance of the matrix around a shear band, since its fundamentally different glassy dynamics alters the macroscopic material response. The loss of correlation within four hours at room temperature in both samples states is remarkable, considering the fact that the samples aged already for more than 200 days at ambient conditions. Therefore, the as-cast bulk MG exhibits a certain amount of

structural activity at zero applied stress and room temperature, and is not structurally frozen [33]. The enhanced relaxation dynamics around the shear-band core clearly demonstrates that macroscopic inhomogeneous yielding does not only result in a structural change limited to a nano-scale shear band. Instead, the here revealed data motivates the picture of a micrometer region around the nanometer shear-band core that exhibits a strongly accelerated relaxation in comparison to the as-cast matrix. This affected shear-band zone is, expressed in cross-sectional width, approximately three orders of magnitude larger than the length scales typically derived from shear-band thickness measurements. A change in the dynamics that only occurs in the shear-band core would not be detectable with the method used here due to the small fraction of the shear band volume in comparison the illuminated volume. Therefore an enhanced structural mobility is not only restricted to the nanoscopic shear-band center but present in a field extending tens of micrometers around the shear-band core.

A. Temperature dependence of the $g_{2,plat}$

The value of $g_{2,plat}$ expresses the height of the intensity correlation function before a decay sets in that typically is related to α-relaxation. Figure 3b displays a general decrease of $g_{2,plat}$ with temperature, which is a direct signature of increased motion (mean-square displacements) of the atoms during the heating protocol. This signature of increasingly less defined atomic position with temperature is equivalent to the known linear decay of the height of first peak in a scattering experiment [57]. The initial offset between the as-cast and the deformed specimen in terms of $g_{2,plat}$ suggests that fast processes cause larger mean-square displacements in the region around the shear-band core than seen in the as-cast state. Giordano and Ruta [51] attributed the decay of $g_{2,plat}$ in a Pd-based glass to a faster relaxation process that cannot be measured directly with XPCS, but the strength of which will determine the decrease of the initial plateau. In parallel, Ref. [51] reports that x-ray scattering reveals a structural change related to an increase in medium-range order (MRO) during the isotherms. A change in the MRO in a MG is linked to re-orientation of local bonding and compaction of the structure, the analysis of which has played a determining role in the understanding of structural mechanisms in glasses and liquids [58-61], and also in the initiation of strain localization [62]. The XPCS data of the present study does not allow quantifying changes in MRO, but the different evolution of $g_{2,plat}$ of the as-cast MG and the material in the shear-band vicinity (Fig. 3b) suggests that the strength of the by Ref. [47] postulated fast relaxation process are different in both samples. This indicates that the material probed around the shear-band core is in a structurally different state than the as-cast MG and that the deformation enables relaxation processes that are either different in type or intensity. We observe that $g_{2,plat}$ of the as-cast MG has

an approximately constant decay rate across the entire studied temperature range. In contrast, the material around the shear-band core exhibits non-trivial variations in the evolution of $g_{2,plat}$, until both samples are reaching a very similar value in the temperature range of 530-544 K. This non-monotonous behavior of $g_{2,plat}$ near the shear-band must be a superposition of increased thermal motion and relaxation, as also has been inferred from in-situ scattering experiments during heating of a ball-milled Pd-glass [57]. If thus the temperature-dependent $g_{2,plat}$ value indeed is linked to another underlying faster relaxation processes (may it be γ- [63,64], or β-relaxations [65]), it is concluded that its intensity varies in the material around the shear-band core. The precise structural origin of this different behavior of $g_{2,plat}$ remains unknown, but it is well established that thermally-induced structural dynamics in binary model glasses [61] and glassy ZrCuAl [59,66] does promote icosahedral cluster formation, and that shear-banding disrupts the icosahedral network [27]. Thus, the very different evolution of $g_{2,plat}$ for the two glassy states investigated, indicates that strain localization via nano-scale shear-banding alters the structure far beyond the core of the shear bands and also enhances fast relaxation dynamics. A faster relaxation dynamics is in agreement with the data displayed in Fig. 3a. Both materials attain a similar $g_{2,plat}$ after a sufficient long annealing protocol at ca. $0.93 \times T_g$ (Fig. 3b,), indicating a similar magnitude of the underlying dynamics.

B. Temperature dependence of the shape parameter

In the past few decades there has been an extensive debate regarding the origin of stretched exponential behavior in the supercooled liquid [67]. As pointed out earlier, the macroscopic response of $\beta < 1$ has either been attributed to a heterogeneous distribution of local exponential relaxation times, or to a homogeneous distribution of stretched exponential relaxation times [67-69]. Furthermore, a compressed exponential decorrelation ($\beta > 1$) in MGs has been linked to a fundamental change of the glassy dynamics, where a crossover from diffusive motion of dynamical heterogeneities [70] to an internal stress relaxation regime occurs [51]. The data presented in Fig. 3c shows, however, the opposite: the value of shape parameter for the stress-biased matrix around the shear-band core remains consistently below or equal to the value observed for the as-cast reference glass. Consequently, stress relaxation cannot be the primary mechanism causing an enhanced value of β in the glass state. In particular when considering that recent results show a long-range stress signature around a shear band [34,35,37,38]. The as-cast glass reveals a compressed exponential decorrelation for all temperatures above ambient conditions with an approximately constant level of β, which is in agreement with previous studies [40,53]. This behavior is not seen for the material around the shear-band core. Instead, the shape parameter of the material around the shear-band core first

rises from ca. 1 to ca. 1.6 in the temperature interval from 304 to 450 K, after which β decays as a function of increasing temperature back to approximately unity.

At ambient conditions, β is equivalent for both material states. This can be understood based on the elapsed time between casting the material or deforming the material and the XPCS experiment. Due to the large elapsed time at that temperature, relaxation has taken place to the extent that the material can be well described by a heterogeneous distribution of local aging times, where each local region is well described with a pure exponential decay (β = 1) [67]. Increasing the temperature initiates time-dependent relaxation, i.e. aging, and while the correlation function decays the relaxation behavior changes. Therefore, one cannot simply assume the same picture as at high temperatures in the supercooled region with an exponential decay of the correlation function of a given local region. In the following, we will identify the influence of aging on the correlation function in order to better understand the behavior of the shape parameter for the material in the shear-band vicinity.

To this end, we determined the normalized correlation functions $(g_2(t,t_w)-1)/g_{2,plat}$ from the TTCFs starting from different waiting times $t_{w,i}$, with i = 1, 2, 3, 4, and scaled them at different temperatures. Here, we use the scaling form for the global correlation function $(g_2(t,t_{w,i})-1)/g_{2,plat} = f[h(t)/h(t_{w,i})]$, with the scaling function $h(t)$. The function f describes the graph of the collapsed correlation function. Figure 6a shows a perfect collapse (Variance $V(\Delta t) = 1.1\cdot10^{-3}$, see Section II.C for details) of correlation functions of different $t_{w,i}$ at T = 304 K, using the most basic scaling function $h(t) = t$. This scaling function is indicative for simple aging and also reflects, in agreement with the findings in Fig. 5b, that the aging behavior around the shear-band core has already slowed down due to the elapsed time between shear deformation and the scattering experiment. Figure 6b shows a scaling of the correlation functions at T = 350 K using the function $h(t) = t$. It is noticeable that the correlation functions do not collapse on a single master curve ($V(\Delta t) = 4.0\cdot10^{-2}$) and clear deviations are noticeable at small values of $h(t)/h(t_{w,i})$ as well as at large ones. Figure 6c shows that the same graphs can be scaled much better when using the function $h(t) = \exp(A\cdot t^{\alpha})$ ($V(\Delta t) = 3.3\cdot10^{-3}$), which is similar to the one used in Ref. [71] with A = 0.02 and α = 0.65. At 450 K, where the shape parameter now decays, an ideal collapse is found using the function $h(t) = \ln(A\cdot t^{\alpha})$ (A = 100, α = 1.9, $V(\Delta t) = 1.3\cdot10^{-3}$) as shown in Fig. 6d, and at 500 K, $h(t) = \ln(A\cdot t^{\alpha})$ (A = 60, α = 1.5, $V(\Delta t) = 9.7\cdot10^{-3}$) excellently describes the aging.

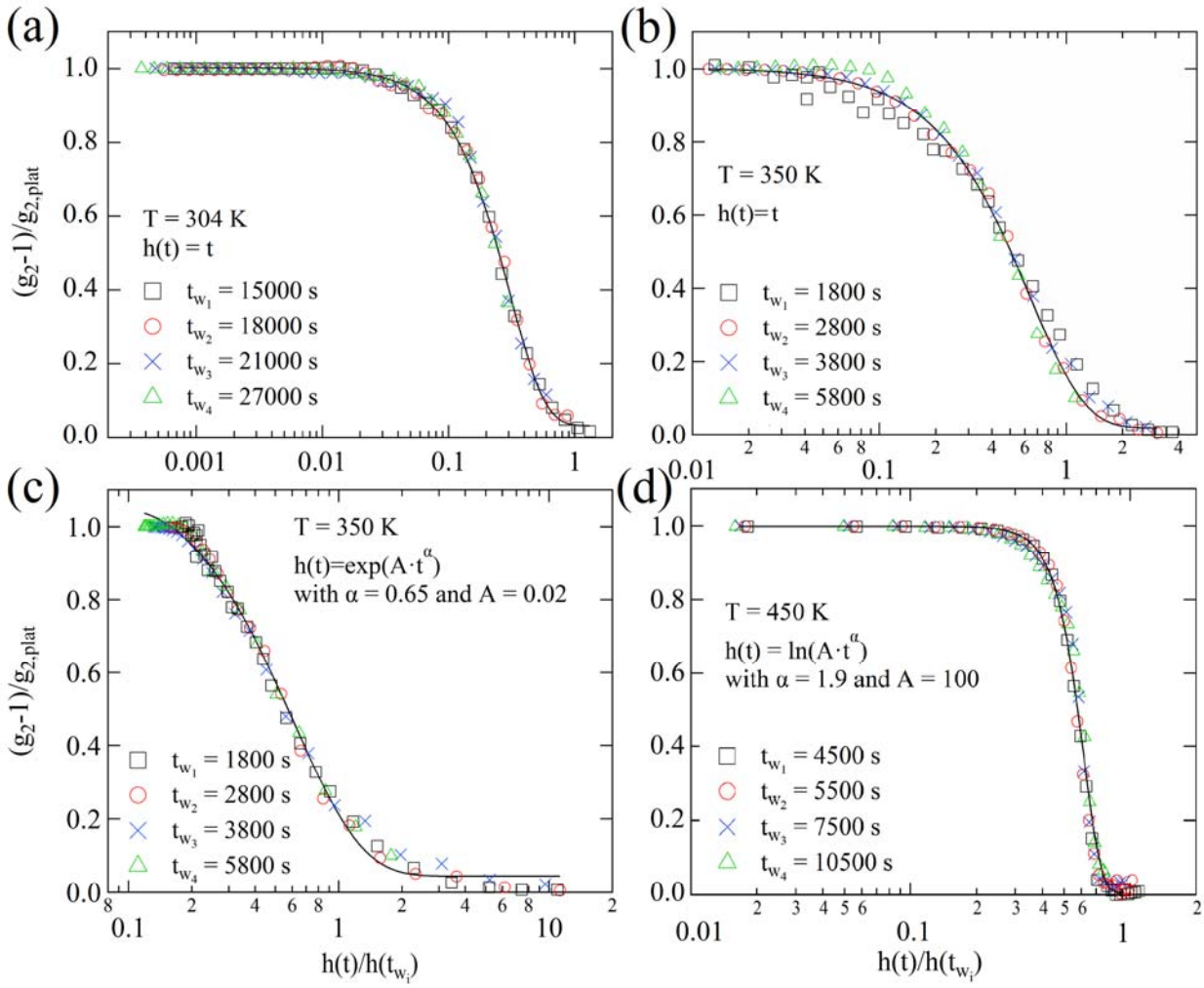

Fig. 6. (a) Collapse of the correlation function at T = 304 K using $h(t) = t$, (b) Collapse of the correlation function at T = 350 K using $h(t) = t$, (c) Collapse of the correlation function at T = 350 K using $h(t) = \exp(A \cdot t^{\alpha})$ with $\alpha = 0.65$ and $A = 0.02$. (d) Collapse of the correlation function at T = 450 K using $h(t) = \ln(A \cdot t^{\alpha})$ with $\alpha = 1.9$ and $A = 100$. Solid black lines originate from the fit function $f(x) = y_0 + B \cdot \exp(-2 \cdot (x/\tau)^{\beta})$. All graphs are for aging behavior of the material around the shear-band core.

Previously, it was shown that scaling via t/τ leads to a good collapse of the correlation function $(g_2\text{-}1)/g_{2,plat}$ of an as-cast Mg-based MG at all temperatures [53]. This result however only holds when the shape parameter remains unchanged, as is approximately the case of the as-cast MG. The exponential (T = 350 K) and the logarithmic (T = 450 and 500 K) scaling forms of $h(t)$ used for the best collapse imply that the shape parameter of the material in the shear-band vicinity in fact undergoes a change from initially being well-described with an exponential scaling, to a second stage of logarithmic scaling, and eventually to a linear scaling, i.e. $h(t) = t$. This means, we are assigning the linear scaling at room temperature to a late stage of aging for the material around the

shear-band core, because the deformed sample has experienced ambient conditions for 10 days. The same applies to the as-cast state. Conducting the identical analysis as outlined above for the material around the shear band, the as-cast material reveals a consistent signature of un-resolvable aging during the isotherms or simple aging, the latter of which is exemplified for 423 K in Figure 7 ($V(\Delta t) = 1.3 \cdot 10^{-3}$). This leads to the conclusion that the shear-band affected zone exhibits a three-stage aging regime, with a change in the aging dynamics as a function of temperature that follows the observed evolution of the shape parameter obtained from the time-averaged relaxation dynamics. We thus speculate that a much longer waiting time at each temperature would have eventually lead to a similar cross-over in aging behavior as here observed as a function of a stepwise heating protocol. Future efforts are needed to substantiate this proposition.

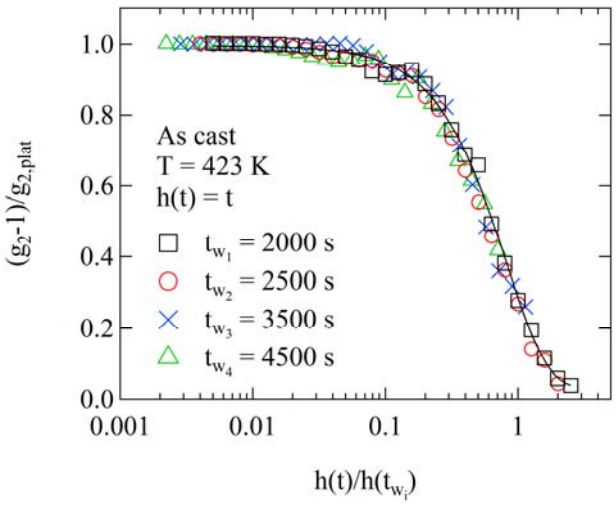

Fig. 7. (a) Collapse of the correlation function at T = 423 K using $h(t) = t$ for the as-cast material.

V. Summary

In conclusion, spatially resolved XPCS measurements around a nano-scale shear band in metallic glasses reveal enhanced structural relaxation processes over a probed length-scale that is about three orders of magnitude larger than the core of the shear band. The relaxation times obtained from time-averaged relaxation behavior are up to one order of magnitude smaller for the material around the shear-band core. The temperature-dependent evolution of the initial value of the intensity correlation function indicates a significantly different structural dynamics (presumably the re-establishment of an icosahedral network) around the shear-band core, if compared to the as-cast reference material. Taking into account time-dependent aging of the metallic glass during heating, it is found that the

aging behavior of the material around the shear-band core undergoes a change between distinctly different aging dynamics, whereas the aging dynamics in the as-cast glass remains well described by simple aging. These experimental findings provide insights into how strain localization via shear banding affects the structure and aging dynamics micrometers away from the shear-band core.

Acknowledgement

This research was carried out in part at the Frederick Seitz Materials Research Laboratory Central Research Facilities, University of Illinois. The authors thank A. Sandy for technical assistance during the beamtime and providing the data analysis software. This research was performed at beamline 8-ID-E of the Advanced Photon Source, a U.S. Department of Energy (DOE) Office of Science User Facility operated for the DOE Office of Science by Argonne National Laboratory under Contract No. DE-AC02-06CH11357. A. Beaudoin is gratefully acknowledged for sharing his mechanical testing set-up. S.K. thanks Karina E. Avila for fruitful discussions. R.M. thanks P.M. Derlet for critical discussions and is grateful for start-up funds provided by the Department of Materials Science and Engineering at UIUC.

References

[1] P. Forsyth, Acta Metallurgica **11**, 703 (1963).
[2] P. Donovan and W. Stobbs, Acta Metallurgica **29**, 1419 (1981).
[3] A. Greer, Y. Cheng, and E. Ma, Materials Science and Engineering: R: Reports **74**, 71 (2013).
[4] T. C. Hufnagel, C. A. Schuh, and M. L. Falk, Acta Materialia **109**, 375 (2016).
[5] R. Maass and J. F. Löffler, Advanced Functional Materials **25**, 2353 (2015).
[6] G. Wilde and H. Rösner, Applied Physics Letters **98**, 251904 (2011).
[7] H. Rösner, M. Peterlechner, C. Kübel, V. Schmidt, and G. Wilde, Ultramicroscopy **142**, 1 (2014).
[8] J. Li, Z. L. Wang, and T. Hufnagel, Physical Review B **65**, 144201 (2002).
[9] Y. Zhang and A. Greer, Applied Physics Letters **89**, 071907 (2006).
[10] C. Liu, V. Roddatis, P. Kenesei, and R. Maass, Acta Materialia **140**, 206 (2017).
[11] H. Chen, Y. He, G. Shiflet, and S. Poon, Nature **367**, 541 (1994).
[12] V. Schmidt, H. Rösner, M. Peterlechner, G. Wilde, and P. M. Voyles, Physical Review Letters **115**, 035501 (2015).
[13] I. Binkowski, G. Shrivastav, J. Horbach, S. Divinski, and G. Wilde, Acta Materialia **109**, 330 (2016).
[14] D. Klaumünzer, A. Lazarev, R. Maass, F. Dalla Torre, A. Vinogradov, and J. Löffler, Physical Review Letters **107**, 185502 (2011).
[15] D. Tönnies, K. Samwer, P. Derlet, C. Volkert, and R. Maass, Applied Physics Letters **106**, 171907 (2015).

[16] W. J. Wright, M. Samale, T. Hufnagel, M. LeBlanc, and J. Florando, Acta Materialia **57**, 4639 (2009).
[17] W. J. Wright, R. R. Byer, and X. Gu, Applied Physics Letters **102**, 241920 (2013).
[18] H. Chen, J. Huang, S. Song, T. Nieh, and J. Jang, Applied Physics Letters **94**, 141914 (2009).
[19] S. Song and T. Nieh, Intermetallics **17**, 762 (2009).
[20] R. Maass, D. Klaumünzer, and J. Löffler, Acta Materialia **59**, 3205 (2011).
[21] R. Maass, D. Klaumünzer, G. Villard, P. Derlet, and J. Löffler, Applied Physics Letters **100**, 071904 (2012).
[22] R. Maass, D. Klaumünzer, E. Preiß, P. Derlet, and J. Löffler, Scripta Materialia **66**, 231 (2012).
[23] E. R. Homer, Acta Materialia **63**, 44 (2014).
[24] Y. Shi and M. L. Falk, Physical Review Letters **95**, 095502 (2005).
[25] Y. Shi and M. L. Falk, Acta materialia **55**, 4317 (2007).
[26] J. Luo and Y. Shi, Acta Materialia **82**, 483 (2015).
[27] A. Cao, Y. Cheng, and E. Ma, Acta Materialia **57**, 5146 (2009).
[28] J. Lewandowski and A. Greer, Nature Materials **5**, 15 (2006).
[29] S. K. Slaughter, F. Kertis, E. Deda, X. Gu, W. J. Wright, and T. C. Hufnagel, APL Materials **2**, 096110 (2014).
[30] P. Thurnheer, F. Haag, and J. Löffler, Acta Materialia (2016).
[31] J.-O. Krisponeit, S. Pitikaris, K. E. Avila, S. Küchemann, A. Krüger, and K. Samwer, Nature Communications **5** (2014).
[32] C. Herrero-Gómez and K. Samwer, Scientific Reports **6** (2016).
[33] J. Bokeloh, S. V. Divinski, G. Reglitz, and G. Wilde, Physical Review Letters **107**, 235503 (2011).
[34] R. Maass, K. Samwer, W. Arnold, and C. Volkert, Applied Physics Letters **105**, 171902 (2014).
[35] R. Maass, P. Birckigt, C. Borchers, K. Samwer, and C. Volkert, Acta Materialia **98**, 94 (2015).
[36] I. Binkowski, S. Schlottbom, J. Leuthold, S. Ostendorp, S. Divinski, and G. Wilde, Applied Physics Letters **107**, 221902 (2015).
[37] A. Vinogradov, M. Seleznev, and I. S. Yasnikov, Scripta Materialia **130**, 138 (2017).
[38] H. S. Shahabi, S. Scudino, I. Kaban, M. Stoica, B. Escher, S. Menzel, G. B. Vaughan, U. Kühn, and J. Eckert, Acta Materialia **111**, 187 (2016).
[39] O. Shpyrko, Journal of Synchrotron Radiation **21**, 1057 (2014).
[40] B. Ruta, Y. Chushkin, G. Monaco, L. Cipelletti, E. Pineda, P. Bruna, V. M. Giordano, and M. Gonzalez-Silveira, Physical Review Letters **109**, 165701, 165701 (2012).
[41] P. Lunkenheimer, R. Wehn, U. Schneider, and A. Loidl, Physical Review Letters **95**, 055702 (2005).
[42] E. Rabani, J. D. Gezelter, and B. Berne, Physical Review Letters **82**, 3649 (1999).
[43] J. Phillips, Reports on Progress in Physics **59**, 1133 (1996).
[44] A. Fluerasu, A. Moussaïd, A. Madsen, and A. Schofield, Phys. Rev. E **76**, 010401 (2007).
[45] R. Bandyopadhyay, D. Liang, H. Yardimci, D. Sessoms, M. Borthwick, S. Mochrie, J. Harden, and R. Leheny, Physical Review Letters **93**, 228302 (2004).
[46] L. Cipelletti, S. Manley, R. Ball, and D. Weitz, Physical Review Letters **84**, 2275 (2000).
[47] L. Cipelletti, L. Ramos, S. Manley, E. Pitard, D. A. Weitz, E. E. Pashkovski, and M. Johansson, Faraday Discussions **123**, 237 (2003).
[48] S. Küchemann, G. Gibbins, J. Corkerton, E. Brug, J. Ruebsam, and K. Samwer, Philosophical Magazine Letters, 1 (2016).
[49] Y. Chushkin, C. Caronna, and A. Madsen, Journal of Applied Crystallography **45**, 807 (2012).
[50] G. Williams and D. C. Watts, Transactions of the Faraday Society **66**, 80 (1970).
[51] V. Giordano and B. Ruta, Nature Communications **7** (2016).

[52] Y. P. Mitrofanov, M. Peterlechner, I. Binkowski, M. Y. Zadorozhnyy, I. S. Golovin, S. V. Divinski, and G. Wilde, Acta Materialia **90**, 318 (2015).
[53] B. Ruta, G. Baldi, G. Monaco, and Y. Chushkin, Journal of Chemical Physics **138**, 054508 (2013).
[54] V. Lubchenko and P. G. Wolynes, Journal of Chemical Physics **121**, 2852 (2004).
[55] Z. Evenson, B. Ruta, S. Hechler, M. Stolpe, E. Pineda, I. Gallino, and R. Busch, Physical Review Letters **115**, 175701 (2015).
[56] E. Vincent, J. Hammann, M. Ocio, J.-P. Bouchaud, and L. F. Cugliandolo, in *Complex Behaviour of Glassy Systems* (Springer, 1997), pp. 184.
[57] N. Mattern, M. Stoica, G. Vaughan, and J. Eckert, Acta Materialia **60**, 517 (2012).
[58] P. J. Steinhardt, D. R. Nelson, and M. Ronchetti, Physical Review B **28**, 784 (1983).
[59] H. Sheng, W. Luo, F. Alamgir, J. Bai, and E. Ma, Nature **439**, 419 (2006).
[60] K. Lad, N. Jakse, and A. Pasturel, Journal of Chemical Physics **136**, 104509 (2012).
[61] P. M. Derlet and R. Maass, Journal of Materials Research **32**, 2668 (2017).
[62] P. M. Derlet and R. Maass, Acta Materialia **143**, 205 (2018).
[63] S. Küchemann and R. Maass, Scripta Materialia **137**, 5 (2017).
[64] Q. Wang, J. J. Liu, Y. F. Ye, T. T. Liu, S. Wang, C. T. Liu, J. Lu, and Y. Yang, Materials Today **20**, 293 (2017).
[65] H.-B. Yu, W.-H. Wang, and K. Samwer, Materials Today **16**, 183 (2013).
[66] Y. Cheng, E. Ma, and H. Sheng, Physical Review Letters **102**, 245501 (2009).
[67] R. Richert, Journal of Physics: Condensed Matter **14**, R703 (2002).
[68] R. Richert, Journal of Non-crystalline Solids **172**, 209 (1994).
[69] M. D. Ediger, C. Angell, and S. R. Nagel, Journal of Physical Chemistry **100**, 13200 (1996).
[70] M. D. Ediger, Annual Review of Physical Chemistry **51**, 99 (2000).
[71] J.-P. Bouchaud, L. F. Cugliandolo, J. Kurchan, and M. Mézard, Spin Glasses and Random Fields, 161 (1998).